# Role of $\pi$-Bonding for Trigonal Level Splittings in Chromium(III) Complexes. 4. Doublet States and Zeeman Level Splittings in $[Cr(bpy)_3]^{3+}$ †

**Thomas Schönherr,*,‡ Michail Atanasov,§ and Andreas Hauser**||

Institut für Theoretische Chemie, Heinrich-Heine-Universität Düsseldorf, Universitätsstrasse 1, D-40225 Düsseldorf, Germany, Institute of General and Inorganic Chemistry, Bulgarian Academy of Science, 1040 Sofia, Bulgaria, and Institut für anorganische und physikalische Chemie, Universität Bern, Freiestrasse 3, CH-3000 Bern 9, Switzerland

*Received February 9, 1995*⊗

A detailed analysis of Zeeman splittings of highly resolved spin-forbidden transitions in $[Cr(bpy)_3](PF_6)_3$ is presented. Assignments of vibronic bands are made based on low-temperature absorption, emission, and infrared spectra. The pattern of doublet states, obtained for H = 0 and H = 5 T, is consistent with angular overlap model (AOM) calculations, which allow one to consider $\sigma$- and $\pi$-interactions between the metal-d and relevant ligand orbitals and the particular angular geometry of the chromophore simultaneously. The observed level splittings are found to result from the combined effect of trigonal distortion and contributions of the symmetry adapted $d_\pi$-orbitals involved due to coupling with corresponding counterparts from the bidentate ligand (*phase coupling*). The larger splitting of the lowest excited state $^2E_g(O_h)$ in the analogous $ClO_4^-$ salt is due to the more distorted geometry of the $[CrN_6]$ moiety. Related properties of the bipyridine ligand, which turn out to show donor behavior in the present compounds, and the acetylacetonate ligand are discussed, and AOM parameters for the metal−ligand $\pi$-interaction are correlated with results of MO calculations.

## 1. Introduction

The nature of the lowest excited states in chromium(III) complexes has been subject of enormous research efforts by physicists and chemists ever since the detection of the R-lines in ruby by Bequerel.[4] This exceptional interest is due to the fact that the photochemical and photophysical behavior is controlled by the level sequence of the excited states, which are well known (by experiment and theory) for compounds containing $Cr^{3+}$ chromophores.[5,6] In the case of $[Cr(bpy)_3]^{3+}$, bpy = 2,2′-bipyridine, however, the overlap of d−d bands with low-lying charge-transfer bands has so far prevented reliable assignments for the two familiar quartet transitions.[7] Likewise, information on the low-lying spin-forbidden transitions, $^4A_{2g} \rightarrow {}^2E_g$, $^2T_{1g}$, has been poor until recently, when Hauser et al.[8] reported highly resolved optical spectra of neat crystalline and doped materials. However, their theoretical treatment in terms of the conventional ligand field theory (LFT) did not consider the specific $\pi$-bonding effects, which are expected to be large for complexes with bipyridine ligands.[9,10] Moreover, the influence of the actual molecular geometry was not explicitly considered. The availability of new X-ray data on $[Cr(bpy)_3](PF_6)_3$[11] prompted us to reinvestigate the energy level scheme in view of the predictions of a more flexible theoretical approach, the angular overlap model (AOM), which takes explicit account of the angular coordination geometry. A further extension, recently introduced into the formalism of the AOM, considers phase relations in extended $\pi$-electron systems of chelating ligands. The so-called *phase coupling* effect may also be of importance for the present bpy complex, leading to three-center ligand field contributions to the *d*-orbital energies.[12] This effect has been successfully applied to acetylacetonate complexes of first-row transition metals.[1−3] Therefore, it is of interest to see whether the extended AOM is also able to explain the low energy states resulting from the $t_{2g}^3$ electron configuration for $[Cr(bpy)_3]^{3+}$, which are fairly well separated from the higher energy charge-transfer states. Particular emphasis will be placed on the detailed assignments of Zeeman transitions. The resulting energy level scheme will be compared with predictions obtained from the conventional and the nonadditive ligand field approach. Finally, we will discuss related properties of the bipyridine and the acetylacetonate ligand and show how the relevant AOM parameters for describing $\pi$-bonding properties can be analyzed by considering the $\pi$-MO's of ligator molecules.

## 2. Optical Transitions

The prominent bands (R-lines) separated by 19.5 $cm^{-1}$ in the absorption spectrum of crystalline $[Cr(bpy_3)](PF_6)_3$ have been unambiguously identified as the zero-phonon transitions into the trigonal split levels $\bar{E} < \bar{2A}$ of the octahedral parent state $^2E_g$.[8] According to Kramers' theorem, all eigenstates of a

† For parts 1−3 in this series, see refs 1−3.
‡ Heinrich-Heine-Universität Düsseldorf.
§ Bulgarian Academy of Science.
|| Universität Bern.
⊗ Abstract published in *Advance ACS Abstracts,* February 15, 1996.

(1) Atanasov, M. A.; Schönherr, T.; Schmidtke, H.-H. *Theor. Chim. Acta* **1987**, *71*, 59.
(2) Schönherr, T.; Atanasov, M. A.; Schmidtke, H.-H. *Inorg. Chim. Acta* **1987**, *141*, 27.
(3) Atanasov, M. A. Schönherr, T. *Inorg. Chem.* **1990**, *29*, 4545.
(4) Becquerel, A. E. *La lumière, ses causes et ses effects*; Gauthier-Villars: Paris, 1867.
(5) Hoggard, P. E. *Coord. Chem. Rev.* **1986**, *70*, 85.
(6) Schönherr, T. In Electronic and Vibronic Spectra of Transition Metal Complexes. 2. In *Topics in Current Chemistry*; Yersin, H., Ed.; Springer: Berlin, in press.
(7) König, E.; Herzog, S. J. *Inorg. Nucl. Chem.* **1970**, *32*, 585.
(8) Hauser, A.; Mäder, M.; Murugesan, R.; Robinson, W. T.; Ferguson, J. *Inorg. Chem.* **1987**, *26*, 1331.
(9) Ceulemans, A.; Bongaerts, N.; Vanquickenborne, L. G. In *Photochemistry and Photo-physics of Coordination Compounds*; Yersin, H., Vogler, A., Eds.; Springer: Berlin, 1987.
(10) Hoggard P. E.; Lee, K.-W. *Chem. Phys.* **1989**, *135*, 219.
(11) Goodwin, K. V.; Pennington, W. T.; Petersen, J. D. *Inorg. Chem.* **1989**, *28*, 2016.
(12) Ceulemans, A.; Dendooven, M.;Vanquickenborne, L. G. *Inorg. Chem.* **1985**, *24*, 1153.

0020-1669/96/1335-2077$12.00/0 

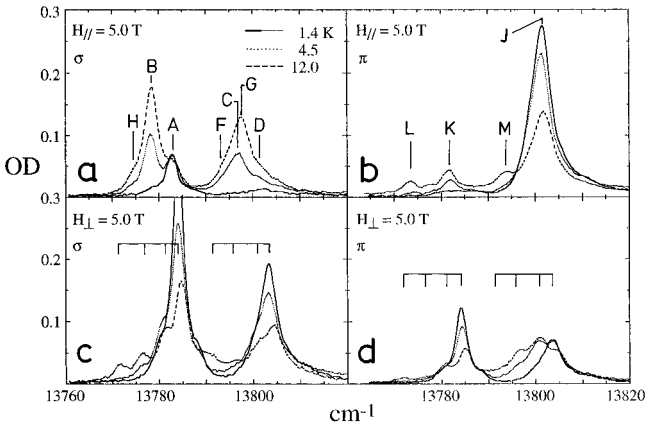


**Figure 1.** Polarized Zeeman spectra in the region of $^4A_{2g} \rightarrow {}^2E_g$ zero-phonon transitions. The capital letters in (parts a and b) refer to Figure 2; the spacings in (parts c and d) are due to the ground state splitting (*see text*).

**Table 1.** Electric Dipole Selection Rules for $^4A_{2g} \leftrightarrow {}^2E_g$ Transitions in Trigonal $d^3$-Systems under the Effect of an External Magnetic Field $H_{||}$ Aligned Parallel to the Molecular $C_3$ Axis (from Ref 17)

| | $^2E_g$ | | | |
|---|---|---|---|---|
| $^4A_{2g}$ | $\overline{E}_{-1/2}$ | $\overline{E}_{+1/2}$ | $\overline{2A}_{-1/2}$ | $\overline{2A}_{+1/2}$ |
| $\overline{E}_{+1/2}$ | $\pi/6$ | $\sigma_0/6$ | $\sigma_1/12$ | $\sigma_0/6$ |
| $\overline{E}_{-1/2}$ | $\sigma_0/6$ | $\pi/6$ | $\sigma_0/6$ | $\sigma_1/12$ |
| $\overline{2A}_{+3/2}$ | | $\sigma_1/4$ | | $\pi/2$ |
| $\overline{2A}_{-3/2}$ | $\sigma_1/4$ | | $\pi/2$ | |

system with an odd number of electrons are at least 2-fold degenerate. Therefore, two spin−orbit states of $\overline{2A}$ and $\overline{E}$ symmetry (using the notation of the underlying $D_3$* double group) are obtained for the $M_S = \pm 3/2$ and the $M_S = \pm 1/2$ components of the $^4A_{2g}$ ($O_h$) ground state, respectively. Selection rules for the electronic transitions $^4A_{2g} \leftrightarrow {}^2E_g$, which are under the regime of a static electric dipole mechanism, are given in Table 1, where $\sigma$ and $\pi$ correspond to a light polarization with electric vector perpendicular and parallel to the molecular $C_3$ axis, respectively. When applied to the transition into the higher $\overline{2A}$ ($^2E_g$) level ($R_2$), the zero-field splitting (zfs) of the ground state, i.e.

$$D(^4A_{2g}) = \overline{2A}_{\pm 3/2}\,(^4A_{2g}) - \overline{E}_{\pm 1/2}\,(^4A_{2g}) = 2D \qquad (1)$$

($2D$ is the zfs parameter commonly used in EPR) can be derived from the slightly different band positions in the polarized absorption spectra: Figure 5a of ref 8 shows the band maximum of $R_2$ to be shifted by 0.8 $cm^{-1}$ to lower energy in the $\sigma$-polarized spectrum reflecting the ordering $\overline{2A} < \overline{E}(^4A_{2g})$ in accordance with the value of $-0.82$ $cm^{-1}$ from a Boltzmann analysis.[8] The zfs of the $^2E_g$ state, which is defined by

$$D(^2E_g) = \overline{2A}_{\pm 1/2}(^2E_g) - \overline{E}_{\pm 1/2}(^2E_g) \qquad (2)$$

is calculated from the separation of R-lines corrected for the zfs of the ground state to $+18.7$ $cm^{-1}$.

An external magnetic field removes Kramers' degeneracies by splitting the states into two components that have opposite values of $M_S$. Figure 1 shows some highly resolved Zeeman spectra of $^4A_{2g} \rightarrow {}^2E_g$ electronic origins in $\sigma$- and $\pi$-polarization measured at temperatures $T = 1.4$, 4.5, and 12 K. Although complicated band patterns are obtained by varying temperature and magnetic field, there is a straightforward way for obtaining definite band assignments for *all* observed spectral features due to zero-phonon transitions. For example, with a magnetic field

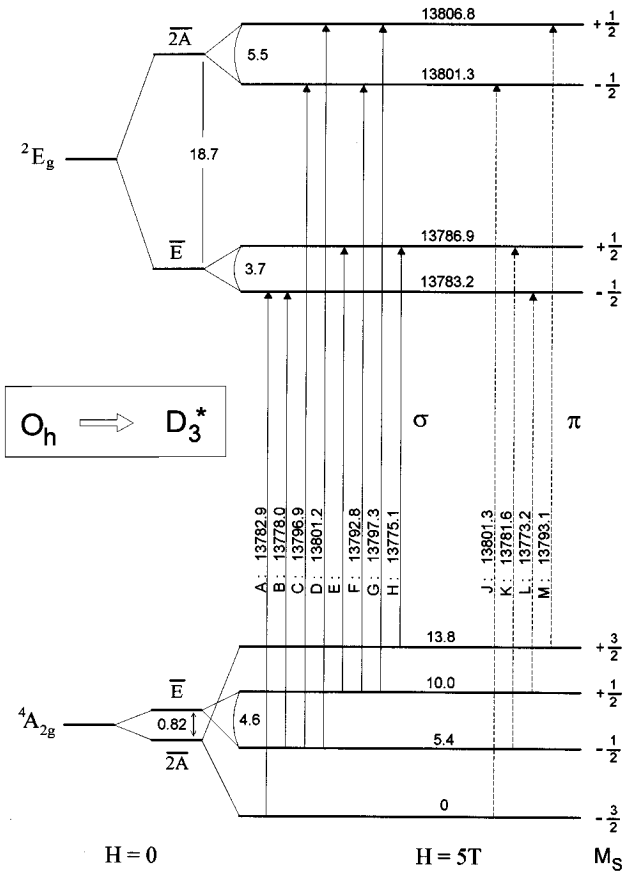


**Figure 2.** Energy eigenvalues and experimentally obtained transition energies due to the $^4A_{2g}$,$^2E_g$ split levels in a magnetic field of $H_{||} = 5$ T.

of 5 T applied parallel to the molecular trigonal axis, just one prominent absorption band appears in $\sigma$-polarization at $T = 1.4$ K (*cf.* Figure 1a). At this temperature, only the lowest component of the ground state manifold is populated to any extent. Thus the peak at 13 782.9 $cm^{-1}$, denoted as A, is readily identified as the $\overline{2A}_{-3/2}(^4A_{2g}) \rightarrow \overline{E}_{-1/2}(^2E_g)$ transition, since transitions from $\overline{2A}_{-3/2}$ to other states resulting from $^2E_g$ are forbidden in $\sigma$. The small features located at 13 778.0 (B) and 13 796.9 $cm^{-1}$ (C) grow rapidly with increasing temperature, showing that these transitions originate from a higher level of the ground state manifold. The comparable band intensities suggest assignments to transitions from $\overline{E}_{-1/2}$ ($^4A_{2g}$) into $\overline{E}_{-1/2}(^2E_g)$ and $\overline{2A}_{-1/2}(^2E_g)$, respectively, both induced by a dipole strength of $\sigma_o/6$ (*cf.* Table 1). This is confirmed by the related spectrum in $\pi$-polarization, which is given in Figure 2b: only one band, denoted as J, appears at $T = 1.4$ K, which is readily identified as the $\overline{2A}_{-3/2}(^4A_{2g}) \rightarrow \overline{2A}_{-1/2}(^2E_g)$ transition. The peak position of J, 13 801.3 $cm^{-1}$, should be equal to the energy of A + C − B. With a value of 13 801.8 $cm^{-1}$, this is within experimental accuracy.

In $\pi$-polarization, selection rules predict three further Zeeman transitions appearing at higher temperatures, and in fact, a total of three bands, K, L, and M, are resolved in the spectrum measured at $T = 12$ K. Its temperature behavior proves band K to be a transition originating from the second ground state level, $\overline{E}_{-1/2}(^4A_{2g})$. According to Table 1, this assignment provides the position of the second component of $\overline{E}$ ($^2E_g$), i.e. $\overline{E}_{+1/2}$. The energy difference 13 781.6 $cm^{-1}$ (K) − 13 778.0 $cm^{-1}$ (B) locates it around 3.5 $cm^{-1}$ higher in energy than $\overline{E}_{-1/2}(^2E_g)$. This ordering for the split levels of $^2E_g(O_h)$ is in accordance with theoretical predictions on the Zeeman splittings

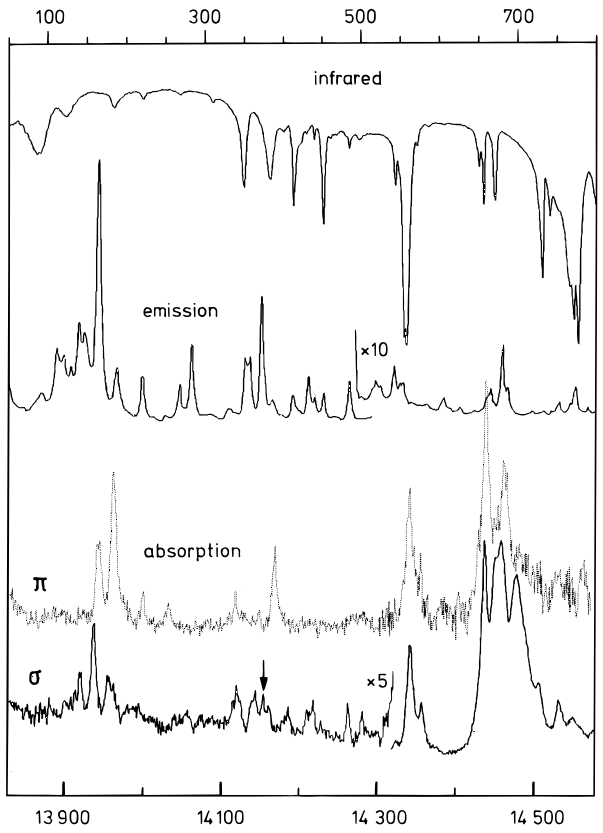


**Figure 3.** Polarized absorption ($T = 1.4$K), emission ($T = 1.4$ K) and infrared spectra ($T = 10$ K) in the 50−800 $cm^{-1}$ region of vibrational transitions. Emission is due to the upper scale using $\nu_{oo}-\nu$ with respect to the zero phonon transition $\nu_{oo} = 13\,778$ $cm^{-1}$ in the [Rh] doped compound.[8] The arrow marks the lowest origin of $^2T_{1g}$ in the $\sigma$-polarized absorption spectrum (*see text and Table 2*).

in trigonally distorted chromium(III) compounds.[13] The energy level diagram showing all electric-dipole allowed $^4A_{2g} \rightarrow {}^2E_g$ transitions observed for $H_{||} = 5$ T is presented in Figure 2. The remaining transitions, D − H, are now easily identified in Figure 1a,b. For example, line L in the $\pi$-spectrum corresponds to the $\bar{E}_{+1/2}(^4A_{2g}) \rightarrow \bar{E}_{-1/2}(^2E_g)$ transition as it picks up intensity only at $T = 12$ K. This assignment determines the Zeeman splitting of $\bar{E}(^4A_{2g})$ to be 4.6 $cm^{-1}$ from the energy difference B − L, as expected with $g_{||}(^4A_{2g}) = 1.986$.[8]

The effect of a magnetic field perpendicular to the trigonal axis on the absorption band pattern is shown in Figure 1c,d. Here only the ground state splitting is resolved in either polarization, showing analogous level sequences over ∼13 wavenumbers as indicated by arrows in the figures. There is in fact no indication of any sizable Zeeman-splitting in the excited state; consequently, the value for $g_\perp$ must be close to zero for both Kramers' doublets resulting from $^2E_g$.

Transitions into states which derive from $^2T_{1g}(O_h)$ are expected a few hundred wavenumbers higher in energy. Figure 3 shows the $\sigma$- and $\pi$-polarized absorption bands in the region 13 800−14 600 $cm^{-1}$ together with related transitions obtained from low-temperature emission and infrared measurements. Locating further electronic origins is complicated by the fact that almost all observed peaks can be identified with vibrational sidebands of one of the origins of $^2E_g$. Table 2 collects the respective assignments showing only the 14 034 and 14 160 $cm^{-1}$ lines having no counterpart in the emission or infrared spectrum. We assign the higher band (arrow in Figure 3) to the lowest spin−orbit component of $^2T_{1g}$, which turned out to be of $\bar{E}$ symmetry (see below) according to its polarization behavior of $\sigma$-type for the corresponding low-temperature transition $\overline{2A}(^4A_{2g}) \rightarrow \bar{E}(^2T_{1g})$. The other two zero-phonon transitions into the trigonally split levels of $^2T_{1g}$ may be located around 14 450 $cm^{-1}$ for the following reasons: (i) a Gaussian band deconvolution of the broad absorption shape shows some additional weak transitions here, which are covered under the intense vibrational sidebands (due to the prominent 657 and 671 $cm^{-1}$ modes) upon both electronic origins; (ii) applying a magnetic field perpendicular to the $C_3$ axis leads to surprisingly high intensities at 14 440 $cm^{-1}$ and, less pronounced, at 14 465 $cm^{-1}$, which is illustrated in Figure 9 of ref 8. This increase of intensity for some spin-forbidden transitions may be explained by Zeeman-induced mixing of the doublet states involved with components of close-lying quartet states (either $d^3$ or charge transfer). The latter give rise to more intense spin-allowed transitions.[23]

In the region of $^4A_{2g} \rightarrow {}^2T_{2g}(O_h)$ transition a series of prominent lines has been observed in the polarized absorption spectra (*cf.* Figure 4 in ref 8). The first sharp band located at

**Table 2.** Vibronic Zero-Field Transitions in the Low-Temperature Absorption Spectrum and Related Vibrational Frequencies Observed in Emission[a] and Infrared Spectra

| absorption | | emission | |
|---|---|---|---|
| $\nu$ | $\nu - \nu_{oo}$ | $\nu_{oo} - \nu$ | infrared |
| $\nu = 13778$ ($\sigma$) origin: $\overline{2A}(^4A_{2g}) \leftrightarrow \bar{E}\,(^2E_g)$ | | | |
| $\nu = 13797$ ($\pi$) origin: $\overline{2A}(^4A_{2g}) \leftrightarrow \overline{2A}(^2E_g)$ | | | |
| 13925 | 129 | 129 | 125 |
| 13943 | 165 | 164 | 164 |
| 13961 | | | |
| 13961 | 183 | 186 | 184 |
| 14000 | 222 | 221 | 221 |
| 14034 | ? | | |
| 14126 | 348 | 352 | 351 |
| 14148 | 351 | | |
| 14160 | (origin) | | |
| 14169 | 382 | 386 | 384 |
| 14189 | 382 | | |
| 14191 | 413 | 412 | 414 |
| 14211 | 414 | | |
| 14219 | 441 | 439 | 440 |
| 14263 | 484 | 486 | 485 |
| 14281 | 484 | | |
| 14322 | 544 | 536 | 544 |
| 14341 | 544 | | |
| 14333 | 555 | 550 | 555 |
| 14352 | 555 | | |
| 14337 | 559 | | 559 |
| 14356 | 559 | | |
| 14349 | 571 | 570 | 571 |
| 14368 | 571 | | |
| 14429 | 651 | 651 | 651 m |
| 14448 | 651 | | |
| 14435 | 657 | 664 | 657 s |
| 14454 | 657 | | |
| 14449 | 671 | 670 | 671 s |
| 14468 | 671 | | |
| 14507 | 729 | | 729 w |
| 14526 | 729 | | |
| 14510 | 732 | 733 | 732 s |
| 14529 | 732 | | |
| 14520 | 742 | | 742 m |
| 14539 | 742 | | |
| 14556 | 778 | 779 | 778 |
| 14807 | 1029 | 1010 | 1016, 1023 |
| 14829 | 1051 | 1032 | 1036 |
| 15296 | 1516 | | 1520 |

[a] From the unpolarized emission spectrum of $[Rh(bpy)_3]$ $(PF_6)_3$:$Cr^{3+}$ at $T = 1.4$ K; $\nu_{00} = 13\,777$ $cm^{-1}$.

(13) Dubicki, L. *Comments Inorg. Chem.* **1991**, *12*, 35.

19 999 $cm^{-1}$ is of $\overline{2A}$ character as calculated for the lowest spin−orbit component of $^2T_{2g}$ (see below). Therefore it is plausible to assign this band as the respective electronic origin, which causes several vibronic satellites with vibrational energies of 155, 167, 372, 665, and 768 $cm^{-1}$. The most intense peak in $\sigma$-polarization is located at 20 056 $cm^{-1}$ and may also be assigned to a doublet origin, because sidebands appear at similar frequencies (155, 372, 665 $cm^{-1}$). The peaks at 20 488 and 20 650 $cm^{-1}$, defying assignments to vibronic sidebands of either origin, are candidates for the third spin−orbit component of $^2T_{2g}$. However, since we are finally not able to distinguish between the zero-phonon transitions of doublet, quartet ($^4A_{2g} \rightarrow {}^4T_{2g}$) or low-lying charge transfer states, which also appear in this spectral region, these assignments cannot be established by spectroscopic arguments alone.

## 3. AOM Calculations

As described in detail by Ceulemans et al.,[12] Atanasov et al.,[1] and Schäffer and Yamatera,[14] *nonadditive* contributions to the ligand field potential may occur in complexes with chelate ligands which have an extended $\pi$-electron system. Within the framework of the conventional (*additive*) AOM, the energy matrix for the $\pi$-orbitals contains two antibonding parameters, which describe the $\pi$-interaction in the chelate plane by $e_{\pi c}$ (or $e_{\pi ||}$) and perpendicular to it by $e_{\pi s}$ (or $e_{\pi \perp}$). Following Orgel,[15] this description is not valid when delocalized $\pi$-electrons are involved as, for example, in acetylacetonate or bipyridyl ligands.[12] Considering the respective $\overline{L-M-L}$ moiety, the relevant molecular orbitals can be classified with respect to the $C_2$ axis into symmetric ($\chi$-type) or antisymmetric ($\psi$-type) MO's. Since combination with metal d-functions can take place only within the same symmetry, wave functions have to be transformed to the relevant $C_{2v}$ symmetry to become adequate linear combinations of the usual basis functions:

$$b_1: \quad d_\psi = \sqrt{1/2}(d_{xz} + d_{yz})$$

$$a_2: \quad d_\chi = \sqrt{1/2}(d_{xz} - d_{yz}) \qquad (3)$$

Within this approach, two different $\pi$-parameters describe the out-of-plane interactions between in-phase $\psi$-type ($e_{\pi s}$) and out-of-phase $\chi$-type ($e_{\pi s}'$) metal and ligand orbitals, respectively. These quantities will certainly be dependent on the respective MO energies of the free ligand which are generally different for $\psi$- and $\chi$-type wave functions. The contributions of the HOMO for $\pi$-donor ligands and for the LUMO for $\pi$-acceptor ligands are usually the most important because of the small energy denominators associated with these molecular orbitals. However, consideration of all individual contributions of filled and empty ligand orbitals may be required in some cases (*vide infra*).

AOM calculations have been performed by diagonalizing the full 120 × 120 secular determinant of the $d^3$ system. The underlying AOM matrix for trigonal $M(L-L)_3$ complexes of $D_3$ symmetry, which is supplemented for orbital phase coupling effects, has been published previously.[3] This matrix was implemented into the AOMX program allowing full account of electronic repulsion, spin−orbit coupling, and Zeeman level splittings for arbitrary $d^n$ complexes.[16]

(14) Schäffer, C. E.; Yamatera, Y. *Inorg. Chem.* **1991**, *30*, 2840.
(15) Orgel, L. E. *J. Chem. Soc.* **1961**, 3683.
(16) Adamsky, H. *AOMX-a Fortran computer package for ligand field calculations within the angular overlap model*; Heinrich-Heine-Universität: Düsseldorf, Germany, 1993.

## 4. Orbital Scheme and Ligand Field States

Ligand field calculations on $[Cr(bpy)_3]^{3+}$ have already been performed by Hauser et al.[8] and, in terms of an extended angular overlap model, by Hoggard and Lee.[10] These calculations have required a total of six parameters, which may be varied independently: the Racah parameters $B$ and $C$, the spin−orbit coupling parameter $\zeta$, and three ligand field quantities ($Dq$, $K$, $K'$) or AOM parameters ($e_\sigma$, $e_{\pi s}$, $e_{\pi s}'$), respectively. However, the appearance of low-lying charge transfer bands, which cover the quartet and higher doublet transitions, strongly confine the experimental data basis, confronting us with the problem of overparameterization which can lead to a good fit even for incorrect assignments. Therefore, we begin with a more qualitative discussion, placing the emphasis on relevant geometries and orbital schemes in order to elucidate the physical origins of the measured band splittings.

The polarized optical spectra of $[Cr(bpy)_3](PF_6)_3$ and their changes with magnetic field and temperature variation determine the level ordering for the zfs of the quartet ground state and the first excited doublet state (*cf.* eqs 1 and 2):

$$^4A_{2g}(O_h): \quad \overline{2A} < \overline{E};\ D(^4A_{2g}) = -0.82\ cm^{-1} \qquad (4)$$

$$^2E_g(O_h): \quad \overline{E} < \overline{2A};\ D(^2E_g) = +18.7\ cm^{-1} \qquad (5)$$

As has been shown previously, the ground state zfs in a tris-chelated $[Cr(L\text{-}L)_3]$ compound is predominantly influenced by the trigonal distortion from the $O_h$ geometry rather than by the distinct $\pi$-interaction with either acceptor- or donor-type ligands.[3,13] The theoretical $^4A_{2g}$ sublevel sequence $\overline{2A} < \overline{E}$ ($\overline{E} < \overline{2A}$) was found to be correlated with a trigonally compressed (elongated) geometry. This is reflected by the experimental data for the present compound. The particularly large zero-field splitting of ~0.8 $cm^{-1}$ together with the sequence of the split levels (eq 1) is in agreement with a trigonal compression of the $[CrN_6]$ octahedron by a large deviation of the polar angle $\vartheta = 58°$ from the value for cubic symmetry ($\vartheta_{cub} = 54.74°$).[10]

Information on the $^2E_g$ splitting in trigonally distorted $d^3$ complexes, on the other hand, can be obtained from the familiar relation[17]

$$D(^2E_g) = \overline{2A}(^2E_g) - \overline{E}(^2E_g) = \frac{4}{3}\zeta \frac{\Delta t_2}{^2E_g - {}^2T_{2g}} \qquad (6)$$

where $\Delta t_2$ represents the energy difference between the e-type and $a_1$-type $t_{2g}$-orbitals in a trigonal ligand field. (It should be noted that the effect of mixing $e(t_{2g})$ and $e(e_g)$ orbitals is originally not considered in the definition of $\Delta t_2$.[13]) Combining eqs 5 and 6 implies that $\Delta t_2$ must be negative to explain the measured sequence of the $^2E_g$ split levels. We will now attempt to elucidate in which way this result is influenced by the specific $\pi$-interaction with the bipyridine ligand. As illustrated in Figure 4, the HOMO (LUMO) of bpy is given by an out-of-phase (in-phase) combination of the ligator $\pi$-MO's. Since this phase relation is opposite compared to the frontier orbitals of the acetylacetonate ligand, it was suggested that the inverted $^2E_g$ splitting of $[Cr(bpy)]^{3+}$ with respect to $[Cr(acac)_3]$ is just the result of this difference.[9] However, this effect may be modified by the large trigonal distortion of the $[CrN_6]$ chromophore in $[Cr(bpy)_3]^{3+}$, which contributes considerably to $\Delta t_2$ as well. In order to separate the geometric effect (trigonal distortion) from electronic properties (in-phase or out-of-phase $\pi$-interaction,

(17) Sugano, S.; Tanabe, Y. J. *Phys. Soc. Jpn.* **1958**, *13*, 880.

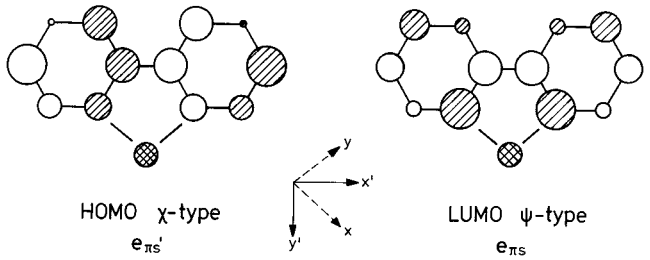


**Figure 4.** Out-of-phase type HOMO and in-phase type LUMO orbitals of bipyridine which are symmetric ($a_2$) and antisymmetric ($b_1$) with respect to the $C_2$ axis.

donor or acceptor behavior), the energy level scheme of the metal d-orbitals is considered first. In a sample calculation, we therefore allowed for positive and negative values of a mean parameter, i.e. $\overline{e_{\pi s}} = (1/2)(e_{\pi s} + e_{\pi s}')$, implying overall donor and acceptor character, respectively, and we examined both types of phase coupling by varying $de_{\pi s}$ ($=e_{\pi s} - e_{\pi s}'$), including the possibility of no phase coupling ($e_{\pi s} = e_{\pi s}'$). Figure 5a shows the energy splittings of the $t_{2g}$-orbitals, $\Delta t_2$, in a contour diagram with $\overline{e_{\pi s}}$ and $de_{\pi s}$ as variables and the other parameters fixed at reasonable values. The experimental value of $D(^2E_g)$, requiring $\Delta t_2 < 0$, immediately excludes in-phase coupling with donor behavior. But the experimental findings can still be qualitatively reproduced by assuming either out-of-phase coupling and overall donor or acceptor properties, or in-phase coupling and overall acceptor character. A $\pi$-acceptor interaction with no phase coupling does also not violate the correct orbital sequence. This is due to the fact that a trigonal compression of the $[CrN_6]$ polyhedron gives a negative contribution for acceptor properties but may result in a positive contribution to $\Delta t_2$ for donor properties of the bpy ligand (Figure 5b).

We have performed a series of AOM calculations on the full $d^3$ system of $[Cr(bpy)_3]^{3+}$. The structural parameters involved, i.e. the angular geometry of the chromophore and the orientations of the chelate planes as given by the angle $\psi$,[3] were taken from refs 11 and 18 for the $PF_6^-$ and the $ClO_4^-$ salts, respectively. Comparison with the experiment was limited to the energy levels originating from the $t_{2g}^3$ electron configuration, because transitions to other states are hidden in the absorption spectrum under very intense charge transfer bands. Our calculations show the splittings of $^2E_g$ and $^2T_{1g}$ to be predominantly influenced by the spin−orbit coupling ($\zeta$) and by the out-of-plane $\pi$-interaction ($\overline{e_{\pi s}}$ and $de_{\pi s}$). In the following $\zeta$ is set to 200 $cm^{-1}$ as estimated from EPR measurements on $[Rh(bpy)_3](PF_6)_3$:$Cr^{3+}$,[8] and the model parameters $B$, $e_\sigma$ and $e_{\pi c}$ are fixed at values known from the AOM analysis of the related pyridine complex.[19] This leaves us with the Racah parameter $C$, which can be adjusted to fit the absolute doublet energies, and $e_{\pi s}$ and $e_{\pi s}'$ as variables. A least-squares fitting procedure based on the Powell algorithm[5] reproduces the experimental energies of $^2E_g$ and $^2T_{1g}$ states (*cf.* section 2) pretty well in terms of negative $e_\pi$ parameters ($\overline{e_{\pi s}} < 0$) and $de_{\pi s}$ close to zero (no phase coupling). This result, which is presented in Table 3, seems in accordance with the alleged $\pi$-acceptor character of the bpy ligand.[9,10] However, since $D(^2E_g)$ is proportional to $\Delta t_2$, there is not just one set of parameters $\overline{e_{\pi s}}$ and $de_{\pi s}$ which reproduces the experimental value of $\sim$19 $cm^{-1}$. This is demonstrated by comparing Figure 5a with a contour plot, which shows a number of isolines for the calculated splittings of $^2E_g$ including the isoline relevant for the specteroscopic findings (Figure 6).

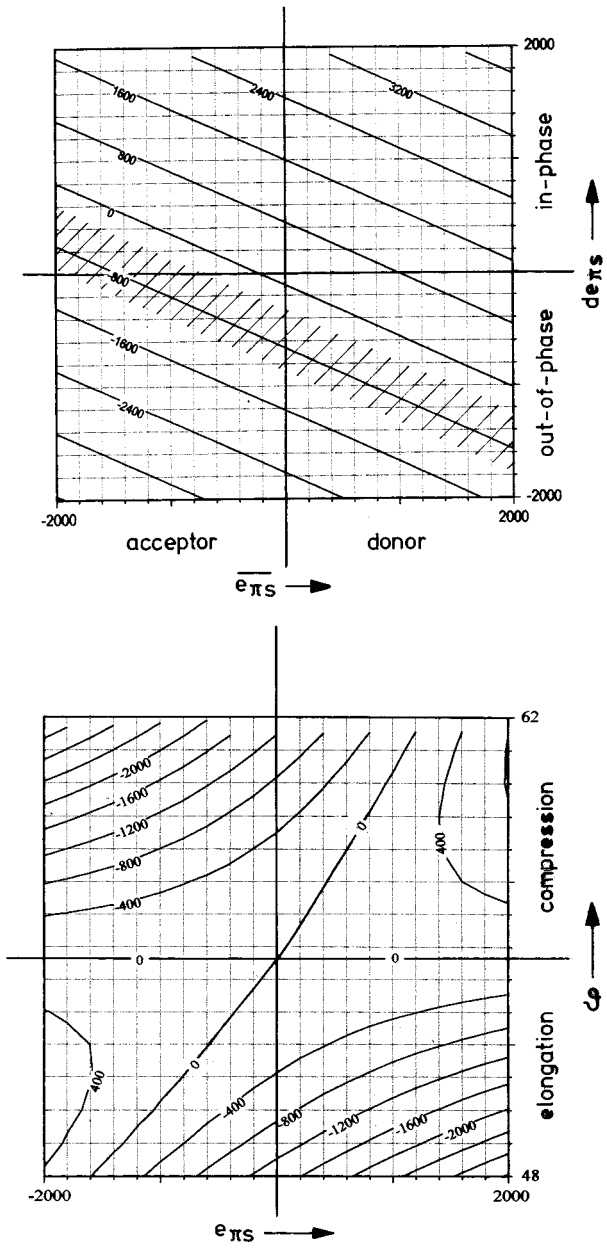





**Figure 5.** Top (a): Contour plot for the $t_{2g}$-orbital splitting of the $PF_6^-$ salt due to the $\pi$- contributions perpendicular to the planes of the bpy ligands. The splitting calculated from eq 6 is within the marked area ($e_\sigma = 8000$ $cm^{-1}$, $\vartheta = 58°$, $\phi = 49.2°$). Bottom (b): Analogous plot with respect to the effect of trigonal distortions versus the (isotropic) $\pi$-behavior of the chromium−bipyridine interaction ($e_\sigma = 8000$ $cm^{-1}$, $\phi = 60°$).

The situation is somewhat different for the $ClO_4^-$ salt, where the molecular geometry of the $[Cr(bpy)_3]^{3+}$ chromophore is much more distorted than for the $PF_6^-$ salt.[18] In accordance with this geometric effect, the $^2E_g$ splitting appears to be distinctly larger (95 $cm^{-1}$ or less) than for the $PF_6^-$ salt (we prefer an alternative interpretation of the excitation spectrum given in ref 18, where the $^2E_g$ splitting is claimed to be $\sim$165 $cm^{-1}$). Figure 6 includes isolines for the $^2E_g$ splitting as a function of $\overline{e_{\pi s}}$ and $de_{\pi s}$ using the structural data for the $ClO_4^-$ salt from ref 18. Assuming that these parameters are the same for both salts, i.e. that the differences in $D(^2E_g)$ are due to geometric impacts only, $\overline{e_{\pi s}}$ and $de_{\pi s}$ should be determined by the crossing point of the $D(^2E_g) = 19$ $cm^{-1}$ isoline in the $PF_6^-$ salt and the respective isoline of the $ClO_4^-$ salt[8] (probably for the value of 95 $cm^{-1}$). However, we are not able to clarify the role of $\pi$-bonding by this procedure yet, because there are two

(18) Lee, K.-W.; Hoggard, P. E. *Polyhedron* **1989**, *8*, 1557.
(19) Schönherr, T.; Degen, J. *Z. Naturforsch.* **1990**, *45A*, 161.

**Table 3.** Observed and Calculated d−d Transition Energies in $[Cr(bpy)](PF_6)_3$ with Parameter Values Fixed[a] ($e_\sigma = 8000$, $e_{\pi c} = 0$, $B = 600$, $\zeta = 200$) and All Data Given in $cm^{-1}$

| assignments | | observed[b] | calculated | |
|---|---|---|---|---|
| | | | *a* | *b* |
| $^4A_{2g}$ | $\overline{2A}$ | 0 | 0 | 0 |
| | $\overline{E}$ | 0.83 | 0.54 | 0.62 |
| | 2*D* | +0.83 | +0.54 | +0.62 |
| $^2E_g$ | $\overline{E}$ | 13 778 | 13 785 | 13 776 |
| | $\overline{2A}$ | 13 797 | 13 805 | 13 795 |
| | *D* | +19 | +20 | +19 |
| $^2T_{1g}$ | $\overline{E}$ | 14 160 | 14 138 | 14 133 |
| | $\overline{2A}$ | 14 437 | 14 442 | 14 472 |
| | $\overline{E}$ | 14 461 | 14 451 | 14 483 |
| | *D* | 301 | 313 | 350 |
| $^2T_{2g}$ | $\overline{2A}$ | 19 999 | 21 538 | 21 156 |
| | $\overline{E}$ | 20 056[c] | 21 638 | 21 211 |
| | $\overline{E}$ | 20 488[c] | 22 180 | 21 526 |
| | *D* | 489 | 642 | 370 |

| fitted param[a] | $\pi$-acceptor[d] | $\pi$-donor[e] |
|---|---|---|
| $e_{\pi s}$ | −950 | 500 |
| $e_{\pi s'}$ | −1000 | 1250 |
| *C* | 3080 | 3100 |

[a] See text. [b] From ref 8. [c] Tentative assignment. [d] $\overline{e_{\pi s}} = -975$, $de_{\pi s} = 50$ (i.e. almost no phase coupling). [e] $\overline{e_{\pi s}} = 875$, $de_{\pi s} = -750$ (i.e. out-of-phase coupling).

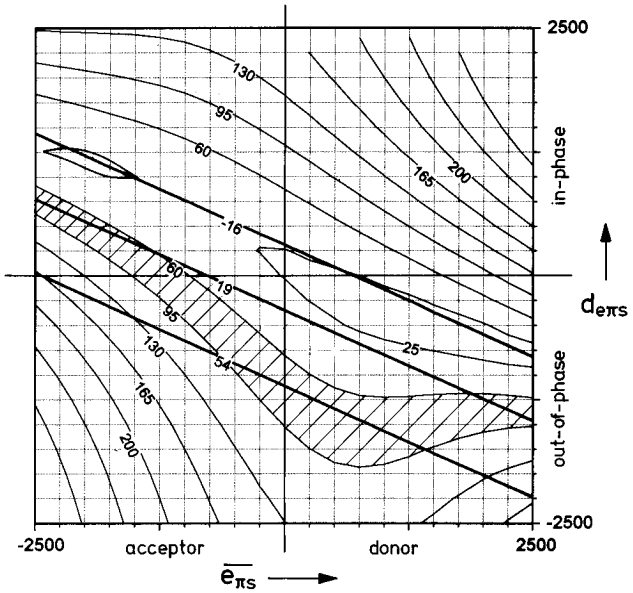


**Figure 6.** Isolines for the energy separation of the $^2E_g$ split levels in the trigonal $PF_6^-$ compound (bold lines) and in the low-symmetry $ClO_4^-$ compound. The experimental values are given with the $19cm^{-1}$ isoline ($PF_6^-$ salt) and in the case of the perchlorate salt by the marked area (uncertain assignment). Other parameters are as in Table 3.

well-suited areas in the parameter space exhibiting rather opposite parameter values. Despite the fact that the solution showing strong acceptor behavior ($\overline{e_{\pi s}} < 0$) resembles the analysis of Hoggard,[10] it will be disregarded on the basis of our EHT-MO calculations (*cf.* section 6). Another possibility presents itself in the region of donor properties and dominating out-of-phase coupling. This solution ($\overline{e_{\pi s}} > 0$, $de_{\pi s} < 0$) is also consistent with the parameters obtained when all observed transition energies are fitted simultaneously. Table 3 compares the experimental transition energies of the low-lying d-states of $[Cr(bpy)_3](PF_6)_3$ with the level schemes calculated on the basis of optimized parameters for the metal−ligand $\pi$-interaction. Because there is good agreement with the experimental results in either case, we are unable to characterize the $\pi$-bonding behavior at the present stage.

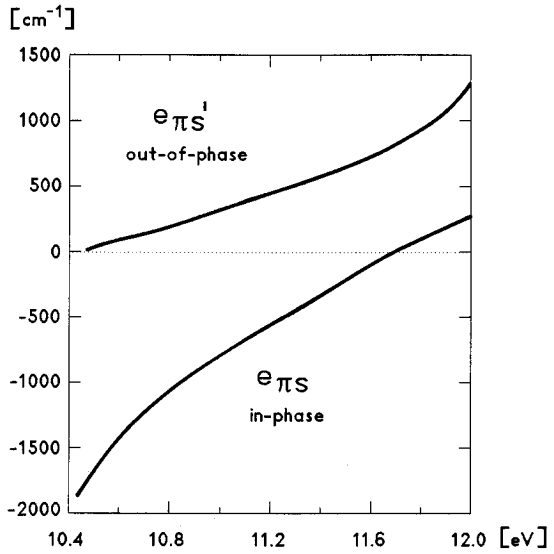


**Figure 7.** Calculated values of the $\pi$-interaction parameters for $[Cr(bpy)_3]^{3+}$ as a function of the free d-orbital energy (*see text*).

**Table 4.** $g_{||}$ Values of $^2E_g$ Sublevels and $^2E_g$ Splitting Calculated under the Influence of Orbital Expansion ($k < 1$) and Trees' Correction ($\alpha > 0$)[a]

Part a

| | expt | calculated | | | |
|---|---|---|---|---|---|
| | | $k = 1$ | $k = 0.8$ | $k = 0.6$ | $k = 0.4$ |
| $g_{||}$ ($\overline{2A}$) | ≈2.4 | 0.8 | 1.1 | 1.3 | 1.5 |
| $g_{||}$ ($\overline{E}$) | ≈1.6 | 3.0 | 2.9 | 2.6 | 2.4 |
| *D* ($^2E_g$) | 19 | 19 | 15 | 11 | 8 |

Part b

| | expt | calculated | | | |
|---|---|---|---|---|---|
| | | $\alpha = 0$ | $\alpha = 100$ | $\alpha = 200$ | $\alpha = 300$ |
| $g_{||}$ ($\overline{2A}$) | ≈2.4 | 0.8 | 1.1 | 1.6 | 2.3 |
| $g_{||}$ ($\overline{E}$) | ≈1.6 | 3.0 | 2.8 | 2.5 | 2.1 |
| *D* ($^2E_g$) | 19 | 19 | 27 | 32 | 29 |
| $^2T_{2g}$−$^2E_g$ | 6400 | 7500 | 7150 | 6800 | 6450 |

[a] The energy separation of $^2T_{2g}$ and $^2E_g$, given also in Part b, is not dependent on *k*. Other parameters as for Table 3. All in $cm^{-1}$.

## 5. Zeeman Splittings

Further insight into the $\pi$-bonding scheme may be obtained by considering the Zeeman splitting of $^4A_{2g}$ and $^2E_g$ states. Applying the Zeeman operator of the form[17]

$$\mathbf{H}_{mag} = \beta H\{\sin\vartheta_{mag}\cos\varphi_{mag}(k_xL_x + 2S_x) + \sin\vartheta_{mag}\sin\varphi_{mag}(k_yL_y + 2S_y) + \cos\vartheta_{mag}(k_zL_z + 2S_z)\} \quad (7)$$

to the real basis functions of $d^3$, values for $g_\perp$ and $g_{||}$ were calculated for each electronic state using the following relation ($\beta = 0.4668\ cm^{-1}\ T^{-1}$)

$$g_{\perp(||)} = \Delta E_{\perp(||)}/\beta H_{\perp(||)} \quad (8)$$

The Zeeman splittings show, as expected, much larger effects for the magnetic field aligned parallel to the trigonal axis. For a magnetic field of $H_{||} = 5$ T the same level sequence of $^2E_g$ split components (defined by pseudo-spin values $-1/2$, $+1/2$) is

**Table 5.** $\pi$-Type MO Energies and Their Composition from Iterative Extended Hückel Calculations on $[Cr(bpy)]^{3+a}$

| no. | energy | type | MO coefficients |
|---|---|---|---|
| 1 | −2.158 | $\chi$ | 0.999 $\phi_1$ |
| | *−2.185* | $\phi_1$ | −0.323 ($p_{z1} - p_{z2}$) + ... |
| 2 | −4.398 | $\psi$ | 0.495 $4p_{z'}$ + 0.878 $\phi_2$ − 0.131 $\phi_6$ |
| | *−4.803* | $\phi_2$ | +0.289 ($p_{z1} + p_{z2}$) + ... |
| 3 | −5.882 | $\psi$ | −0.837 $4p_{z'}$ +0.478 $\phi_2$ − 0.140 $\phi_5$ + 0.269 $\phi_6$ − 0.130 $\phi_{10}$ − 0.142 $\phi_{12}$ − 0.042 $d_{y'z'}$ |
| | *−6.430* | 4p | +1.0 $4p_{z'}$ |
| 4 | −6.664 | $\chi$ | 1.0 $\phi_3$ |
| | *−6.665* | $\phi_3$ | −0.022 ($p_{z1} - p_{z2}$) + ... |
| 5 | −8.404 | $\chi$ | 0.107 $d_{x'z'}$ + 0.997 $\phi_4$ |
| | *−8.452* | $\phi_4$ | −0.364 ($p_{z1} - p_{z2}$) + ... |
| 6 | −8.480 | $\psi$ | 0.053 $d_{y'z'}$ + 0.987 $\phi_5$ |
| | *−8.455* | $\phi_5$ | +0.142 ($p_{z1} + p_{z2}$) + ... |
| 7 | −9.476 | $\psi$ | 0.162 $d_{y'z'}$ − 0.944 $\phi_6$ |
| | *−9.349* | $\phi_6$ | +0.426 ($p_{z1} + p_{z2}$) + ... |
| 8 | −12.415 | $\chi$ | 0.750 $d_{x'z'}$ − 0.632 $\phi_7$ − 0.214 $\phi_9$ − 0.140 $\phi_{11}$ |
| | *−12.700* | *3d* | 1.0 $d_{x'z'}$ |
| 9 | −12.530 | $\psi$ | −0.944 $d_{y'z'}$ − 0.128 $\phi_6$ + 0.081 $\phi_8$ − 0.299 $\phi_{10}$ − 0.156 $\phi_{12}$ |
| | *−12.700* | *3d* | 1.0 $d_{y'z'}$ |
| 10 | −12.669 | $\chi$ | −0.590 $d_{x'z'}$ − 0.774 $\phi_7$ + 0.204 $\phi_9$ |
| | *−12.572* | $\phi_7$ | + 0.117 $\phi_{11}$ +0.140 ($p_{z1} - p_{z2}$) + ... |
| 11 | −13.701 | $\psi$ | 0.993 $\phi_8$ + 0.108 $\phi_{10}$ |
| | *−13.697* | $\phi_8$ | +0.039 ($p_{z1} + p_{z2}$) + ... |
| 12 | −13.809 | $\chi$ | 0.252 $d_{x'z'}$ + 0.956 $\phi_9$ |
| | *−13.725* | $\phi_9$ | +0.324 ($p_{z1} - p_{z2}$) + ... |
| 13 | −14.008 | $\psi$ | −0.260 $d_{y'z'}$ + 0.940 $\phi_{10}$ |
| | *−13.869* | $\phi_{10}$ | −0.347 ($p_{z1} + p_{z2}$) + ... |
| 14 | −15.398 | $\chi$ | −0.136 $d_{x'z'}$ − 0.982 $\phi_{11}$ |
| | *−15.347* | $\phi_{11}$ | −0.436 ($p_{z1} - p_{z2}$) + ... |
| 15 | −16.056 | $\psi$ | −0.108 $d_{y'z'}$ + 0.981 $\phi_{12}$ |
| | *−16.004* | $\phi_{12}$ | +0.369 ($p_{z1} + p_{z2}$) + ... |

[a] The second lines refer to the orbitals of $Cr^{3+}$ and 2,2′-bipyridine (denoted by $\phi_i = 1, ..., 12$) without metal-ligand interaction. Coordinate system choice as given in Figure 4. Only MO-coefficients for d- and p-orbitals of the metal, and for $\pi$-orbitals of ligator atoms are presented. Cr orbital exponents: 4s = 4p, 1.70; 3d, 4.95 (0.50579) + 1.80 (0.67472). Orbital energies (in eV): input $H_{4s} = -8.66$, $H_{4p} = -5.24$, $H_{3d} = -11.22$. Output after charge iteration: $H_{4s} = -10.271$, $H_{4p} = -6.43$, $H_{3d} = -12.696$. Iterated configuration of Cr: $4s^{0.360}4p^{0.216}3d^{4.88}$.

calculated as predicted from the spectroscopic assignments. On the other hand, Zeeman splittings of $\overline{E}(^2E_g)$ and $\overline{2A}(^2E_g)$ are calculated to be rather small (1.3 and 0.4 $cm^{-1}$, respectively) when a magnetic field perpendicular to the trigonal axis is applied. This is again in line with the experiment showing Zeeman splittings spectroscopically not resolved in any case for $H_\perp = 5$ T.

However, the calculated $g_{||}$ values are significantly different for $\overline{E}$ ($g_{||} = 3$) and $\overline{2A}$ ($g_{||} = 0.9$) compared to values of ∼1.6 and ∼2.4, respectively, derived from the absorption spectra. In accordance with our experimental result, Riesen reported $g_{||} = 1.76 \pm 0.01$ for the lowest excited state, $\overline{E}$ ($^2E_g$), from fluorescence line-narrowing measurements.[20] On the other hand, the AOM calculations on $g_{||}$ can be somewhat improved if the Stevens orbital reduction ($k < 1$)[21] and Trees' correction ($\alpha > 0$)[5] are taken into account. Both effects lower $g_{||}(\overline{E})$ and increase $g_{||}(\overline{2A})$ correspondingly as illustrated by the data in Table 4.

### 6. Nature of the Metal−Ligand $\pi$-Bonding

In this section we discuss the various contributions to the $\pi$-bonding parameters derived for the bipyridine complex, and compare them with the recently investigated acetylacetonate complex of chromium(III). For this purpose the perturbation on the metal-centered $d_\pi$-orbitals by the $\pi$-type MO's of bipyridine is explicitly considered. The latter can be divided into occupied (donor) and non-occupied (acceptor) MO's, giving positive and negative contributions to the energies of the corresponding metal functions, respectively. The other classification of these orbitals is given by in- and out-of-phase symmetry properties influencing $e_{\pi s}$ and $e_{\pi s}'$ separately. Therefore, making use of symmetry-adapted d-orbitals (*cf.* Figure 4), we have to consider in total four terms contributing to the out-of-plane metal−ligand $\pi$-interaction:

$$\text{in-phase:} \qquad e_{\pi s}(d_{y'z'}) = e_{\pi s}(\text{donor}) + e_{\pi s}(\text{acceptor})$$

$$\text{out-of-phase:} \quad e_{\pi s}'(d_{x'z'}) = e_{\pi s'}(\text{donor}) + e_{\pi s'}(\text{acceptor}) \qquad (9)$$

The various terms in eq 9 were obtained from a second-order perturbation, using expressions for each of the four possible combinations, which are given, for example, by

$$e_{\pi s}(\text{donor}) = 2H_{p-d\pi}{}^2 \sum_{l,i} c_{li}{}^2/(H_d - H_l) \qquad (10)$$

Here $c_{li}$ is the MO coefficient of the ligand $2p_z$-orbital ($i = 1, 2$) in the corresponding $\pi$-type ligand MO ($l$ numerates the in-phase orbitals only), and ($H_d - H_l$) represents the energy difference between the 3d-orbitals of $Cr^{3+}$ and that MO. Numerical values were evaluated by a standard extended Hückel calculation,[22] where the resonance integral $H_{p-d\pi}$ was set to 0.738 eV using the Wolfsberg-Helmholz approximation. The calculated values of $e_{\pi s}$ and $e_{\pi s}'$ are plotted in Figure 7 as function of the d-orbital energy $H_d$.

(20) Riesen, H. *J. Luminesc.* **1992**, *54*, 71.
(21) Jørgensen, C. K. *Struct. Bonding* **1966**, *1*, 3.
(22) (a) Calzaferri, G.; Forss, L.; Kamber, I. *J. Phys. Chem.* **1989**, 93, 5366. (b) Calzaferri, G.; Brändle, M. Extended Hückel Calculations. *QCPE Bull.* **1992**, *12* (4).
(23) Hensler, G.; Gallhuber, E.; Yersin, H. *Inorg. Chem.* **1987**, *26*, 1641.

The analysis of the various contributions to the $\pi$-interaction show that the energy effect of the ligand p-orbitals on the corresponding metal d-orbitals cannot be due to interactions of HOMO and/or LUMO type alone. In fact, ligand orbitals which are more distant in energy have to contribute considerably to the $\pi$-parameters, i.e. to the ligand field potential acting on the $Cr^{3+}$ ion. Figure 7 shows that the overall $\pi$-bonding function of bpy varies from acceptor to donor depending on the explicit value of $H_d$. This means that contributions of the $\pi$-functions of bpy crucially depend on the position of the metal d-orbitals with respect to the ligand ones. Iterative extended Hückel calculations for the Cr−bpy moiety show that the assumed standard energy $H_d = -11.22$ eV drops on charge iteration to $-12.955$ eV, approaching the HOMO's of the ligand. The respective MO energies and coefficients as well as input and output parameter values are given in Table 5. The MO's orbitals of mainly metal-d character (nos. 8, 9: $d_\chi$, $d_\psi$) are affected mostly by occupied ligand $\pi$-orbitals. As seen from the d-contributions to the MO's of dominant ligand character, $d_\chi$ is primarily influenced by HOMO no. 10, while $d_\psi$ undergoes most perturbation from a lower lying $\psi$ type ligand orbital (no. 13). The EHT calculations thus corroborate the postulated donor properties with dominant out-of-phase $\pi$-interaction, i.e. and $e_{\pi s}' > e_{\pi s} > 0$. It is also seen from the MO's in Table 5 that $d_\chi$ shows a larger covalent reduction than $d_\psi$, which correlates with the $a_1$- and e-type orbitals in the tris-chelated complex.[1] This could serve as explanation for covalent orbital reduction factors $k_z < k_{x,y}$ as well as for orbital quenching by introducing Trees' correction which result from the fitting of the trigonal level splittings in magnetic fields (*cf.* Table 4).

In summary, the bpy ligand was found to act as an out-of-phase $\pi$-donor ligand to $Cr^{3+}$, where the metal−ligand $\pi$-interactions are determined also by more distant energy levels which contribute by means of some larger MO-coefficients, overcompensating the energy denominator in eq 10. This situation has not been explicitly considered for the earlier investigated complex $[Cr(acac)_3]$, where perturbation on the $d_\pi$-levels only by virtue of its HOMO (donor function) have been used in order to explain the energy level scheme.[1,9] Thus we have to check our approximation by using all Hückel MO's of the acac ligand, likewise. Neglecting in first approximation the difference between the carbon and oxygen atoms, the energies for the $\pi$-MO's (in terms of Hückel's parameter $\beta < 0$) and MO-coefficients for the frontier ligand orbitals are readily obtained. Taking the ligand p-orbital energy at zero (O-atom) and denoting the Cr-3d energy by $\Delta$, we calculate the $\pi$-parameters $e_{\pi s}$ and $e_{\pi s}'$ (and the related values of $e_{\pi s}$ and $de_{\pi s}$) as

$$e_{\pi s}(\text{donor}) = 2H_{p-d\pi}{}^2\{{}^1/_3\Delta + 1/[12(\Delta + \sqrt{3}|\beta|)]\}$$

$$e_{\pi s}'(\text{donor}) = 2H_{p-d\pi}{}^2/\{4(\Delta + |\beta|)\}$$

$$e_{\pi s}(\text{acceptor}) = 2H_{p-d\pi}{}^2/\{12(\Delta - \sqrt{3}|\beta|)\}$$

$$e_{\pi s}'(\text{acceptor}) = 2H_{p-d\pi}{}^2/\{4(\Delta - |\beta|)\} \qquad (11)$$

Experimental data show that the ligand-to-metal charge-transfer transitions are at far lower energy than the ligand−ligand transitions, implying $\Delta \ll |\beta|$. Therefore $e_{\pi s}$(donor) clearly dominates, followed by a smaller $e_{\pi s}'$ (acceptor) interaction. In this respect the acac ligand, which causes in-phase perturbation on the $d_\pi$-levels mainly by virtue of its HOMO, can be considered as a rather limiting case. This result is not changed, in fact, when better acac orbitals, e.g. obtained from ab initio calculations, are used.[1]

## 7. Conclusion

The present investigation illustrates that the trigonal level splittings in tris-chelated chromium(III) complexes, as far as reliable experimental data are available, can be rationalized and elucidated within the angular overlap model when symmetry and energy effects of the ligand $\pi$-electrons on the d-levels are appropriately considered. Although low-lying charge transfer states influencing the latter in an unknown way limit applications of the ligand field model, in particular with respect to the numeric accuracy of the calculated energies, the phase coupling concept developed within the AOM approach is shown to be a useful guide to account for extended $\pi$-effects, while preserving the attractive features of the ligand field description.

**Acknowledgment.** This work has been supported by the Bulgarian Academy of Science, the Deutsche Forschungsgemeinschaft and the Alexander-von-Humboldt Foundation. We thank H. Adamsky for some special modifications of the AOMX program. Valuable discussions with Prof. A. Ceulemans and Dr. D. Braun, Katholieke Universiteit Leuven, are acknowledged. The experimental part was performed at the Australian National University, Canberra.

IC950150O